Turkish Journal of Electrical Engineering & Computer Sciences

http://journals.tubitak.gov.tr/elektrik/

Research Article

Turk J Elec Eng & Comp Sci
(2018) 26: 2618 – 2632
© TÜBİTAK
doi:10.3906/elk-1612-122

Path planning and energy flow control of wireless power transfer for sensor nodes in wireless sensor networks

Chenyang XIA[1,*], **Yang ZHANG**[1], **Yuling LIU**[1], **Kezhang LIN**[1], **Jun CHEN**[2]
[1]School of Information and Electrical Engineering, Faculty of Electrical Engineering,
China University of Mining and Technology, Xuzhou, China
[2]Nanjing Nari-Relays Electric Co, Ltd, Nanjing, China

Received: 12.12.2016 • **Accepted/Published Online:** 08.06.2018 • **Final Version:** 28.09.2018

Abstract: In wireless sensor networks (WSNs), limited-capacity batteries are generally used for powering sensor nodes, where unbalanced electricity is the primary cause of premature death of WSNs. In this paper, wireless power transfer networks are used to power batteries in WSNs to avoid the problem of limited lifetime of traditional limited-capacity batteries. Furthermore, path planning based on the Dijkstra algorithm, which aims at minimizing the overall energy consumption in the network to improve system efficiency, is discussed in detail. Finally, three power transfer models with low contention level (LCL) topology for energy flow control are experimentally validated from the optimal path.

Key words: Wireless sensor networks, wireless power transfer networks, path planning, energy flow control

1. Introduction

Wireless sensor networks (WSNs) are integrated intelligent information systems, including information collection, information transmission, and information processing to monitor harsh environmental conditions (temperature, humidity, pressure, etc.) [1,2]. In WSNs, wireless sensor nodes are usually powered by limited-capacity batteries, which results in limited network lifetime. However, network lifetime is a measure of WSNs' main performance indicators. Therefore, the improvement of network lifetime has become a key issue in studies regarding WSNs. Besides, regular replacement of batteries increases economic and labor cost.

In recent years, great effort has been devoted to prolonging network lifetime for WSNs. In terms of sensor and network, it is typical and conventional to reduce the energy consumption in WSNs through low-power hardware architecture, low-complexity software implementation, power-efficient wireless communications, dynamic routing techniques, and mobile data gathering [3–7]. Although these research methods are effective to some degree, network lifetime is still determined by the limited battery energy.

Recently, wireless power transfer (WPT) has emerged as a promising technology to address energy and lifetime bottlenecks in a sensor network. WPT technology, which has advantages of safety, convenience, reliability, and being environmentally friendly and has been widely applied in transportation, medical electronics, and mobile electronic devices [8–10], is employed to supply power to battery in wireless sensor node to avoid its regular replacement. A large number of wireless power transfer nodes constitute wireless power transfer networks (WPTNs) which are widely used in inspection robots, soccer robot competitions, smart homes, and bridge detection.

*Correspondence: bluesky198210@163.com

This work is licensed under a Creative Commons Attribution 4.0 International License.

In [11], Lee proposed a wireless information and power transfer scheme through microwave power transfer such that WSN node can be recovered. Since the battery consumption of a sensor module hindered the development of the bridge health monitoring system, [12] introduced a WPT system controlled by a microchip board which can reduce maintenance cost and extend battery lifespan to be long enough. In [13], a multifunctional mobile entity called SenCar was employed for joint energy replenishment via WPT and data gathering via short-range communication. Some researchers came up with a special WSN powered by radio frequency energy transfer technology. He et al. [14] studied the radio frequency energy provisioning problem in wireless rechargeable sensor networks. They proposed an empirical recharge model based on experimental data. Yan et al. [15] proposed a circuit model for charging and corresponding RF charging time and derived the node lifetime expressions.

WPT technologies employed to supply power to WSNs commonly include inductively coupled power transfer (ICPT), radio frequency (RF), and microwave power transfer (MPT). It was reported in [14] that RF power transfer efficiency is only about 1.5 percent when a receiver is 30 cm away from the energy transmitter. Compared to the ICPT technology, in order to transfer enough energy, RF energy transfer may pose safety concerns for humans. Moreover, RF is used widely, so interference generated by other devices using the same frequency band may lead to severe charging performance degradation. As for MPT, its impact on human body is unknown, and it even causes damage to human body in high power applications when used close to human body. Therefore, in our research, we used the ICPT technology to supply power to WSNs applied on the short- and middle-range occasions. ICPT has a limitation due to the contradiction between the power transfer efficiency and power transmission distance. To provide steady and high recharging rates for power supplies or sensors, a joint design of energy replenishment and data gathering by exploiting mobility is proposed. In our research, relay nodes were employed to help overcome the distance limitation directly, and power was efficiently transferred from a transfer node to a receiver node via relay nodes over a relatively long transmission distance. Besides, we avoided energy consumption during transmission by using an algorithm to find the shortest path.

In summary, WSNs powered by WPTNs, proposed in this paper, can achieve bidirectional transfer of energy and signal. Furthermore, path planning based on the Dijkstra algorithm for searching the optimal path of energy transfer is discussed in detail. Finally, three power transfer models with LCL topology for energy flow control are proposed and verified by experiments.

2. Energy path planning in WPTNs

The structure of WSN node powered by WPTN is shown in Figure 1. Basic components of WSN nodes are the same with those of the traditional structure which consists of a sensor, microprocessor, wireless communication module, and battery. What makes the WSNs in this paper different from the traditional ones is that an additional WPT module is used for charging the battery to overcome the weaknesses of its limited-capacity and unbalanced-electricity.

WPTNs shown in Figure 2 (take 9 nodes as an example) are formed by the massive nodes shown in Figure 1, which can receive or transmit energy. In order to avoid energy consumption during transmission, it is extremely significant to find a simple and reliable algorithm to search for the shortest path for energy transfer. In this paper, we preferred the Dijkstra algorithm by considering efficiency, stability, and timeliness. To obtain the optimal path using an algorithm, WPTNs for WSN nodes can be equivalent to a mathematical model of the abstract weighted chart shown in Figure 3. Consider an undirected graph G $= < V, E >$ with set $V(G)$ of nodes and set E of edges, where $v \in \{v_1, v_2, ..., v_n\}$ and $E = \{E_{ij} \pounds\ i \geq 0, j \geq 0\}$. E_{ij} is the edge of nodes

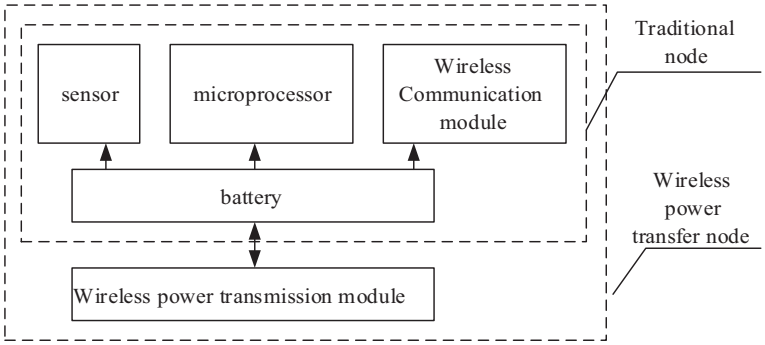

Figure 1. WSN node with wireless power transfer technology.

v_i and v_j, and $f(v_i, v_j)$ is the edge weight.

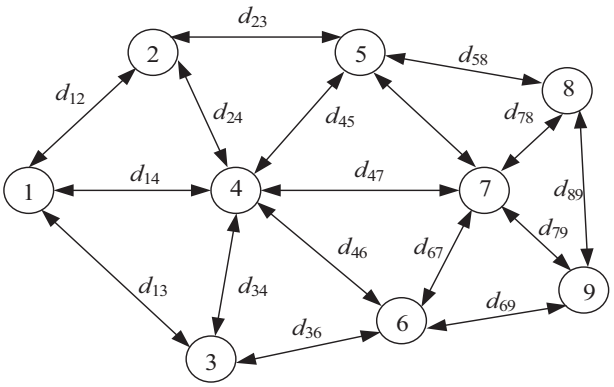

Figure 2. Wireless power transfer networks with 9 nodes.

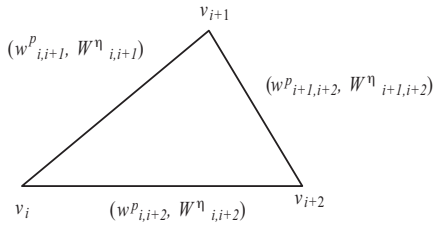

Figure 3. Weighted chart.

Weight matrix A is defined as:

$$A = (d_{ij})_{n \times n}, \tag{1}$$

where

$$d_{ij} = \begin{cases} f(v_i v_j) & if: \exists v_i \to v_j \\ \infty & if: v_i \mapsto v_j \\ 0 & if: i = j \end{cases}.$$

$$d_{ij} = \begin{cases} f(v_i v_j) & E_{ij} \neq 0 \\ \infty & E_{ij} = 0 \\ 0 & i = j \end{cases}$$

The weight d_{ij} is determined by the sum of two nodes' residual energy W^p and transmission efficiency W^η between them. Generally, the larger the W^p is, the stronger the transmission link is and the more residual energy can be obtained. Assuming that γ^p and γ^η represent residual energy of transmission link and weight factor of transmission efficiency respectively, W is the total residual energy of the WPTNs. In total, $f(v_i\, v_j)$ can be expressed as:

$$f(v_i v_j) = \gamma^p(W - W_{ij}^p) + \gamma^\eta(1 - W_{ij}^\eta). \tag{2}$$

Objective optimization function on the path $P = (v_1,\ v_d)$ can be obtained as:

$$f(p(v_1, v_d)) = \sum_{i,j=1}^{d} \gamma^p(W - W_{ij}^p) + \gamma^\eta(1 - W_{ij}^\eta). \tag{3}$$

When it comes to constraint condition,

$$\min f(p(v_1, v_d). \tag{4}$$

Here, v_1 is the initial node and v_d is the target node.

According to the previous analysis, the path planning can be described as a search for a power transfer path $P = (v_1,\ v_d)$ to minimize the value of objective optimization function in the weight graph G. The Dijkstra algorithm, whose more common variant fixes a single node v_s as the "source" node and finds the shortest paths from the source to all the other nodes in the graph producing a shortest-path tree [16], was adopted for path planning. The flowchart is shown in Figure 4.

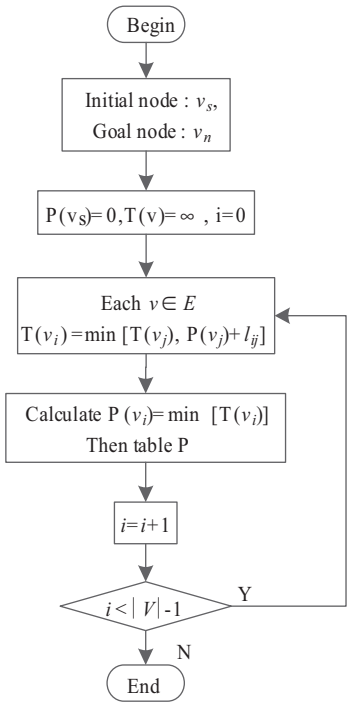

Figure 4. Flowchart of the Dijkstra algorithm.

Programs based on the Dijkstra algorithm in MATLAB implement path planning for finding an optimal path by calculating the residual energy of each node and combining the transmission efficiency and distance of WPT.

The residual energy of each node and transfer efficiency between every two nodes are shown in Tables 1 and 2. Two optimal paths, calculated by the Dijkstra algorithm for energy balance from initial node 1 to target nodes 7 and 9 are shown in Figure 5.

Table 1. Residual energy of each node.

Node	1	2	3	4	5	6	7	8	9
Energy/J	74	62	64	65	70	60	50	58	49

Table 2. Transmission efficiency of each node.

i \ j	1	2	3	4	5	6	7	8	9
1		85.2%	73.5%	76.8%	0	0	0	0	0
2	85.2%		63.5%	83.2%	74.2%	0	0	0	0
3	73.5%	63.5%		88.8%	64.2%	78.2%	66.5%	0	0
4	76.8%	83.2%	88.8%		84.2%	81.9%	76.2%	68.2%	0
5	0	74.2%	64.2%	84.2%		71.2%	74.3%	78.1%	0
6	0	0	78.2%	81.9%	71.2%		83.2%	72.2%	81.2%
7	0	0	66.5%	76.2%	74.3%	83.2%		83.4%	81.2%
8	0	0	0	68.2%	78.1%	72.2%	83.4%		80.3%
9	0	0	0	0	0	81.2%	81.2%	80.3%	

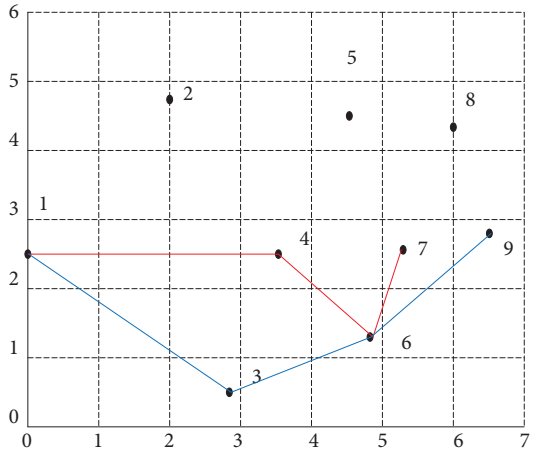

Figure 5. Simulation diagram of path planning.

The optimal path can achieve energy balance for all the nodes in WSNs under the condition of the highest transmission efficiency. Time multiplexing is adopted for energy balance of WSNs, that is, only one condition (transfer of energy or reception of energy) is worked for each node in a period of time.

3. Energy flow control for WPTNs

3.1. Basic models

The three basic energy transfer models in Figure 6 (taking 3 nodes as an example) can be summarized from Figure 5: one-to-multi, multi-to-one, and relay-type.

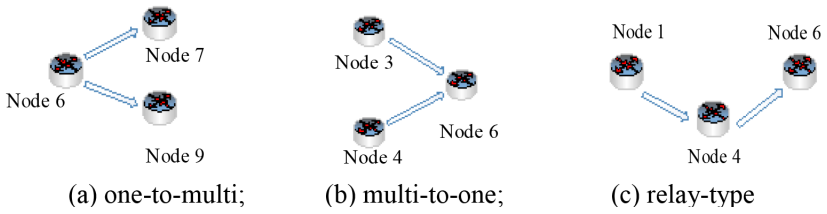

Figure 6. Three basic energy transfer models.

The LCL topology in Figure 7 is used for the nodes of WPTNs because its constant current characteristic makes energy flow control simpler when the resonant angular frequency of each node is:

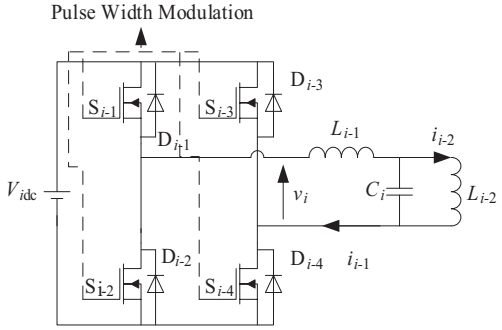

Figure 7. LCL topology of node in WPTNs.

$$\omega_0 = \frac{1}{L_{i-1}C_i} = \frac{1}{L_{i-2}C_i}. \tag{5}$$

In Figure 7, the full-bridge inverter is composed by power switches S_{i-1}-S_{i-4} and their internal free-wheeling diodes D_{i-1}-D_{i-4}, V_{idc} is the battery voltage of WSNs node, V_i is the inverter output voltage, i_{i-1} and i_{i-2} are the charging current and field current respectively, C_i is the compensating capacitor, L_{i-1} and L_{i-2} are the energy transfer coil. Besides, pulse width modulation (PWM) is adopted for energy flow control of all full-bridge inverters in WPTNs. S_i is the trunk link switch which will be closed when node i is a relay node.

Energy bidirectional transmission is the foundation of energy flow control for WPTNs, so one-to-one model in Figure 8 serves as an example to analyze the energy flow control strategy. Assume that node i is the primary node and node j is the secondary node, energy forward transmission is analyzed in detail because one-to-one model is a symmetrical topology. Thus, the proposed bidirectional system can be simplified as an equivalent circuit shown in Figure 9.

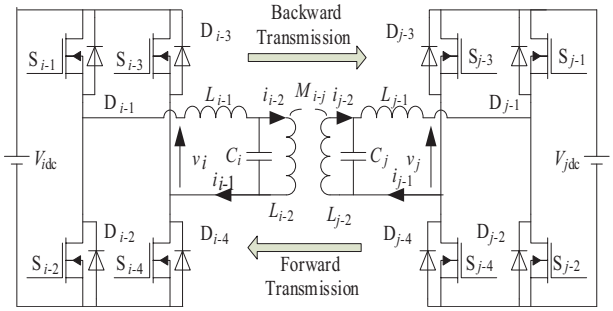

Figure 8. One-to-one model.

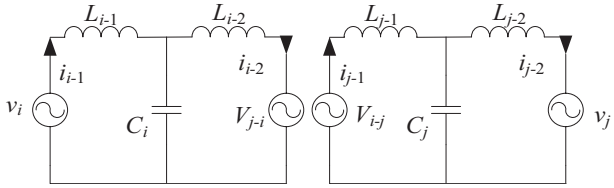

Figure 9. Equivalent circuit of one-to-one model.

The inverter output voltages v_i and v_j can be simplified as a sinusoidal voltage source by neglecting higher order harmonics. Let us assume that v_i and v_j are expressed as follows by the vector method:

$$\dot{V}_i = \sqrt{2}\,|V_i|\,\angle\alpha_i, \tag{6}$$

$$\dot{V}_j = \sqrt{2}\,|V_j|\,\angle\alpha_j, \tag{7}$$

where α_i and α_j are the initial angles of v_i and v_j respectively.

According to the Norton equivalent principle, primary field current I_{i-2} can be expressed as:

$$\dot{I}_{i-2} = \frac{\dot{V}_i}{j\omega_0 L_{i-1}} = \frac{\sqrt{2}\,|V_i|\,\angle(\alpha_i - 90^\circ)}{\omega_0 L_{i-1}}. \tag{8}$$

In the stable case, the induced voltage of node jV_{i-j} is:

$$\dot{V}_{i-j} = j\omega_0 M_{i-j}\dot{I}_{i-2}. \tag{9}$$

From (8) and (9), the induced voltage V_{i-j} can be simplified as:

$$\dot{V}_{i-j} = \sqrt{2}\frac{|V_i|\,M_{i-j}}{L_{i-1}}\angle\alpha_i. \tag{10}$$

The input current I_{j-1} is:

$$\dot{I}_{j-1} = \frac{\dot{V}_{i-j}}{j\omega_0 L_{j-2}} = \frac{\sqrt{2}\,|V_i|\,M_{i-j}}{\omega_0 L_{i-1} L_{j-2}}\angle(\alpha_i - 90^\circ). \tag{11}$$

When the energy is transmitted from node i to node j, the received power P_{i-j} of node j is:

$$P_{i-j} = \frac{1}{T}\int \dot{V}_j \times \dot{I}_{j-1} = \frac{|V_i|\,|V_j|\,M_{i-j}}{\omega_0 L_{i-1} L_{j-2}}\sin\theta_{i-j}. \tag{12}$$

The phase difference θ_{i-j} between different inverter output voltages v_i and v_j is presented in (13):

$$\theta_{i-j} = \alpha_i - \alpha_j \tag{13}$$

From (12), it is evident that the direction of energy flow depends on θ_{i-j}. Thus, a leading phase ($0 < \theta_{i-j} \leq \pi/2$) makes energy flow transmitted from node i to node j, while a lagging phase ($-\pi/2 \leq \theta_{i-j} < 0$) makes energy flow transmitted in opposite directions.

3.2. Power control strategy

From (12), the phase difference θ_{i-j} is usually kept at $\pm\pi/2$ to ensure maximum power transfer and maintain unity power factor at the input end of system. Based on the above analysis, the PWM phase shift control strategy is adopted to adjust the inverter output voltage of all nodes. When there is constant switching frequency and 50% duty cycle for all switches, taking control strategy of node i for example, the relationship between the driving signals of switches S_{i-1}-S_{i-4} and output voltage of the primary inverter is shown in Figure 10, where φ_i is the phase-shifting angle of the inverter which is related to the magnitude of transmission energy.

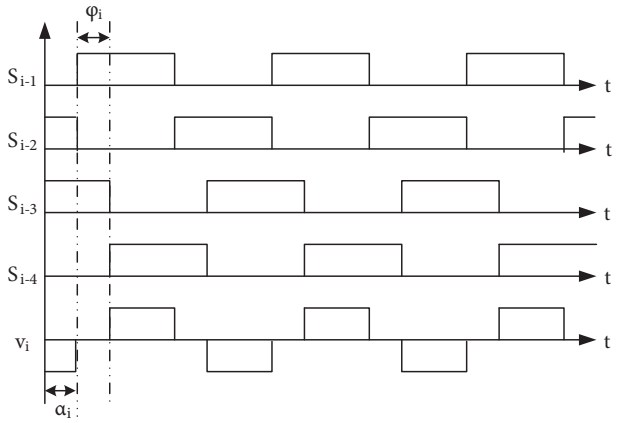

Figure 10. Diagram of phase-shifting control.

S_{i-1} and S_{i-2} are conducted complementarily while S_{i-3} and S_{i-4} are lagging at the phase-shifting angle ϕ_i $(0 \le \phi_i \le \pi)$. The inverter output voltage v_i of node i with the initial phase angle α_i $(0 \le \alpha \le 2\pi)$ can be expressed as follows by FFT:

$$v_i = \sum_{n=1,3,5,\cdots}^{+\infty} V_n \sin\left(n\omega_0 t - \alpha_i\right) = \sum_{n=1,3,5,\cdots}^{+\infty} \frac{4V_{idc}}{n\pi} \cos\left(\frac{n\varphi_i}{2}\right) sin\left(n\omega_0 t - \alpha_i\right). \tag{14}$$

Furthermore, v_i can be expressed as follows by neglecting higher order harmonics:

$$\dot{V}_i \approx \frac{4V_{idc}}{\pi} \cos\left(\frac{\varphi_i}{2}\right) \angle\alpha_i. \tag{15}$$

Similarly, the inverter output voltage v_j of node j with initial phase angle α_j is:

$$\dot{V}_j \approx \frac{4V_{jdc}}{\pi} \cos\left(\frac{\varphi_j}{2}\right) \angle\alpha_j. \tag{16}$$

From (12), (15), and (16), it can be concluded that:

$$P_{i-j} = \frac{\frac{4V_{idc}}{\sqrt{2}\pi} \cos\left(\frac{\varphi_i}{2}\right) \frac{4V_{jdc}}{\sqrt{2}\pi} \cos\left(\frac{\varphi_j}{2}\right) M_{i-j}}{\omega_0 L_{i-1} L_{j-2}} \sin\theta_{i-j}. \tag{17}$$

From (17), for a given circuit and working frequency, the magnitude of transmission power depends on phase difference θ_{i-j}, phase-shifting angles ϕ_i and ϕ_j for the inverters.

4. Power control and modeling for three basic modes

After deeply analyzing the power flow control strategy in Section 3, in this section we will interpret three basic modes shown in Figure 6. The equivalent circuit of the three energy transfer modes has been respectively given in Figure 11, Figure 12, and Figure 13 — one-to-two model, two-to-one model, and relay-type model.

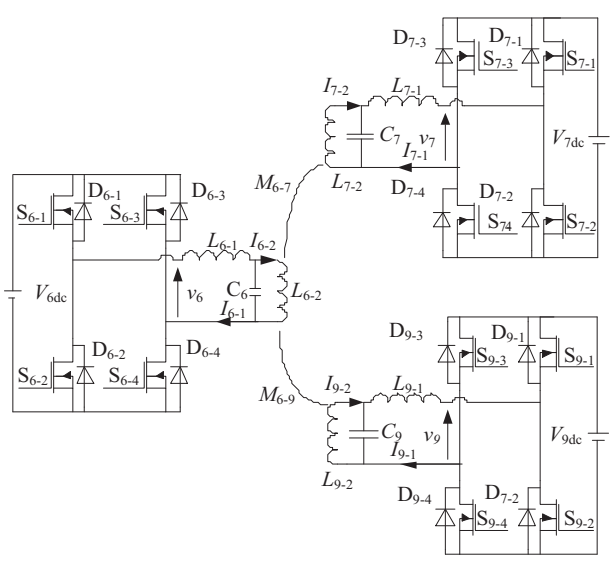

Figure 11. Circuit topology of one-to-two model.

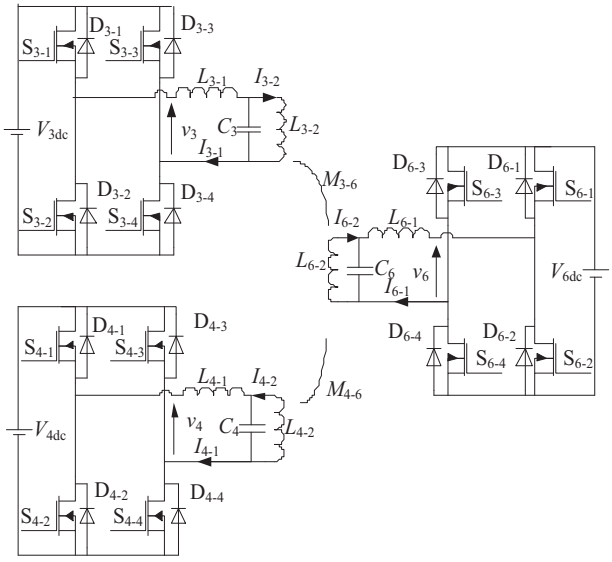

Figure 12. Circuit topology of two-to-one model.

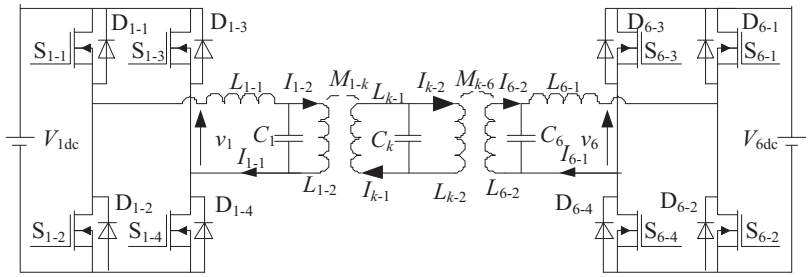

Figure 13. Circuit topology of relay-type model.

For one-to-two model in Figure 11, node 6 is the energy transmitting node and nodes 7 and 9 are the energy receiving nodes. In general, the mutual inductance between node 7 and 9 on the secondary side is usually ignored. Thus, the energy distribution can be realized conveniently by changing the phase-shifting angles ϕ_7 and ϕ_9 of the receiving nodes. Similarly, for two-to-one model in Figure 12, the phase-shifting angles ϕ_3 and ϕ_4 are controllable variables for power control. In relay-type model in Figure 13, the phase-shifting angle ϕ_1 is a controllable variable. The equations of transmission power of three basic models are shown in Table 3.

5. Experiments for energy flow control

The experimental platform for energy flow control is shown in Figure 14. Full-bridge inverter was adopted to control the direction and magnitude of the energy flow. The control circuits of all nodes are composed of two parts: microprocessors and drive circuit, one consists of DSP (TMS320F28335) used for generating pulse and

Table 3. Transmission power and variables for energy flow control of three basic energy flow control models.

Models	Direction	Transmission power	Variables
One-to-two	6→7	$P_{6-7} = \frac{\frac{8V_{6dc}V_{7dc}}{\pi^2}\cos\left(\frac{\varphi_7}{2}\right)M_{6-7}}{\omega L_{6-1}L_{7-2}}\sin\theta_{6-7}$ (18)	φ_7
	6→9	$P_{6-9} = \frac{\frac{8V_{6dc}V_{9dc}}{\pi^2}\cos\left(\frac{\varphi_9}{2}\right)M_{6-9}}{\omega L_{6-1}L_{9-2}}\sin\theta_{6-9}$ (19)	φ_9
Two -to- one	3→6	$P_{3-6} = \frac{\frac{8V_{3dc}V_{6dc}}{\pi^2}\cos\left(\frac{\varphi_3}{2}\right)M_{3-6}}{\omega L_{3-1}L_{6-2}}\sin\theta_{3-6}$ (20)	φ_3
	4→6	$P_{4-6} = \frac{\frac{8V_{4dc}V_{6dc}}{\pi^2}\cos\left(\frac{\varphi_4}{2}\right)M_{4-6}}{\omega L_{4-1}L_{6-2}}\sin\theta_{4-6}$ (21)	φ_4
Relay-type	1→6	$P_{1-4-6} = \frac{\frac{8V_{1dc}V_{6dc}}{\pi^2}\cos\left(\frac{\varphi_1}{2}\right)M_{1-4}M_{4-6}}{\omega L_{1-1}L_{4-1}L_{6-2}}\sin\theta_{1-6}$ (22)	φ_1

the other includes bootstrap circuit with driving chip IR2110. Furthermore, the following experiments were all carried out under forward transmission ($\theta_{i-j} = \pi/2$).

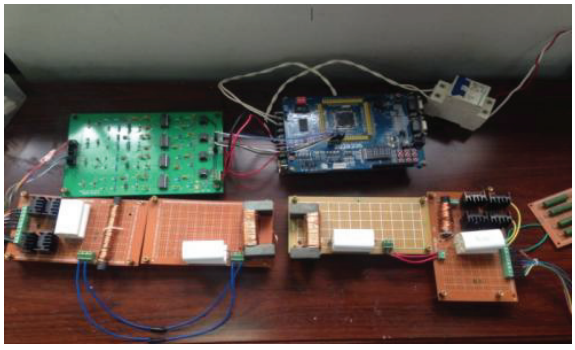

Figure 14. Experimental platform.

5.1. Power bidirectional transmission

According to the parameters in Table 4, an experimental platform is built to verify the feasibility of power bidirectional transmission. Assuming that nodes 1 and 4 are chosen for the experiment of power bidirectional transmission, phase difference θ_{1-4} is equal to $\pi/2$ when energy is transferred from node 1 to node 4.

Table 4. Parameters for all nodes in WPTNs.

Notes	Symbol	Value
Nominal operation frequency	f_0	20 kHz
Input DC voltage	V_{idc}	12 V
Inductance	L_{i-1}, L_{i-2}	105.54 μH
Compensating capacitance	C_i	0.6 μF

In Figure 15, the inverter output voltage v_1 and the charging current i_{1-1} of node 1 are in the same direction, which means node 1 is in the state of energy output. The different direction between the inverter output voltage v_4 and the charging current i_{4-1} shows that node 4 is in the state of energy input. For energy

forward transmission, phase difference θ_{1-4} equals -$\pi/2$ so that the energy can be transmitted from node 4 to node 1. Similarly, node 1 is in the state of energy input and node 4 is in the state of energy output in Figure 16. Moreover, phase-shifting angles φ_1 and φ_4 are both set at 0 degree in the experiments of energy bidirectional transmission.

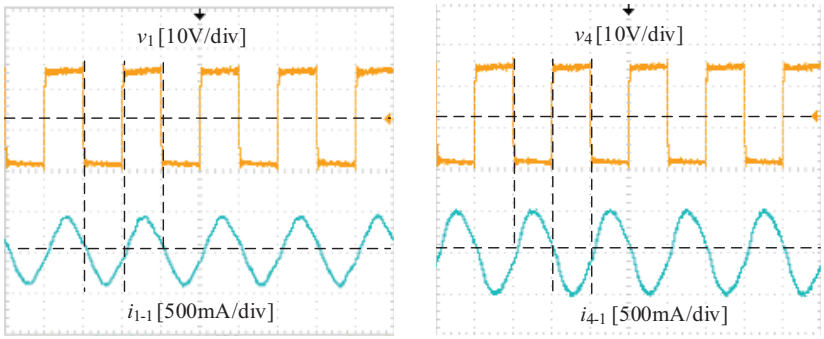

Figure 15. Inverter output voltages and charging currents in one-to-one model.

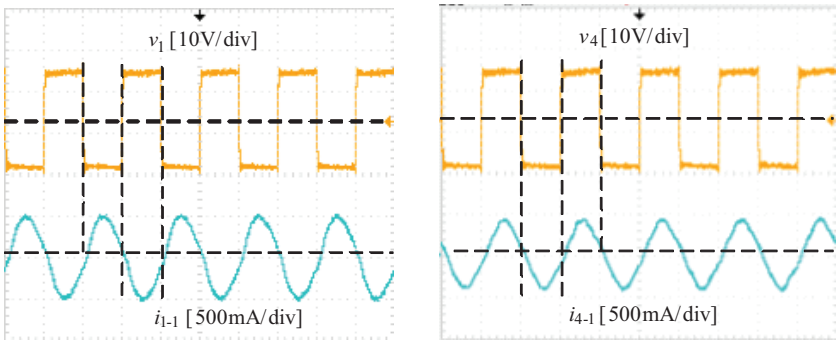

Figure 16. Inverter output voltages and charging currents in one-to-one model.

5.2. One-to-two model

According to Section 5.1, energy can be transmitted bidirectionally between different nodes. In order to balance the energy of nodes in WPTNs, three models and energy flow control strategies have been proposed above. We employed DSP for power control in this paper. Since their use of three modes is similar, we take one-to-two model as an example.

In one-to-two model, in order to balance the remaining energy of the three nodes, node 6 needs to supply power to node 7 and node 9. The values of the phase-shifting angles φ_7 and φ_9 of the energy receiving nodes can be calculated by Eqs. (18) and (19). According to Tables 1 and 3, the relevant parameters used to verify the energy flow control strategy are shown in Table 5.

We use two pairs of complementary PWM waves with dead-time to control the switches of node 6 and then, after 1/4T, the phase-shifting control is used to control the switches of node 7 and node 9, respectively. Since the experiment is carried out under forward transmission ($\theta_{i-j} = \pi/2$), which has already been mentioned in the manuscript, the time of controlling the node 7 and node 9 switches with the DSP board lags behind the time of controlling node 6 (i.e., 1/4T). The PWM waves of controlling node 6 generated by the DSP are shown

Table 5. Parameters for one-to-two model.

Node	Note	Value	
6	Residual energy	60 J	
	Phase-shifting angle ϕ_6	0°	
7	Residual energy	50 J	
	Received power	Theory	3 W
		Reality	2.85 W
	Phase-shifting angle ϕ_7	74.4°	
9	Residual energy	49 J	
	Received power	Theory	4 W
		Reality	3.82 W
	Phase-shifting angle ϕ_9	58.6°	

in Figure 17; the phase-shifting PWM waves of controlling node 7 generated by the DSP are shown in Figure 18; the phase-shifting PWM waves of controlling node 9 generated by the DSP are shown in Figure 19.

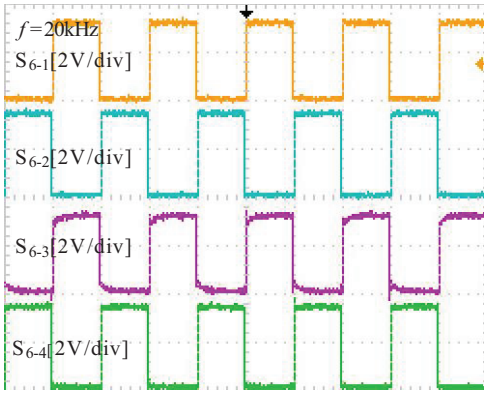

Figure 17. PWM waves of controlling node 6 generated by the DSP.

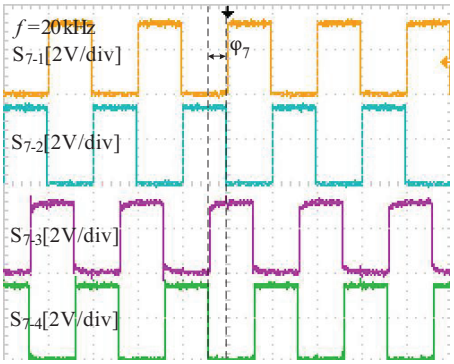

Figure 18. Phase-shifting PWM waves of controlling node 7 generated by the DSP.

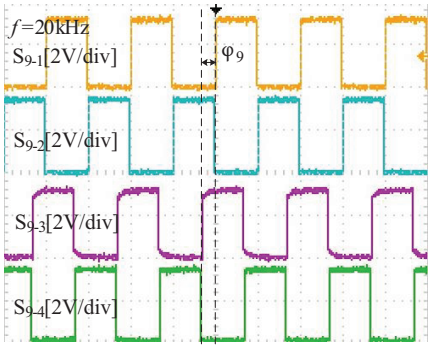

Figure 19. Phase-shifting PWM waves of controlling node 9 generated by the DSP.

Inverter output voltages and charging currents of receiving nodes 7 and 9 are shown in Figure 20. The received powers measured by the power analyzer are 2.85 W and 3.82 W respectively. Parasitic resistances

of coils and capacitance variability are the reasons for error between theory and reality. The inverter output voltage and charging current of the same node are in different directions, which indicates that the node works in the state of receiving power.

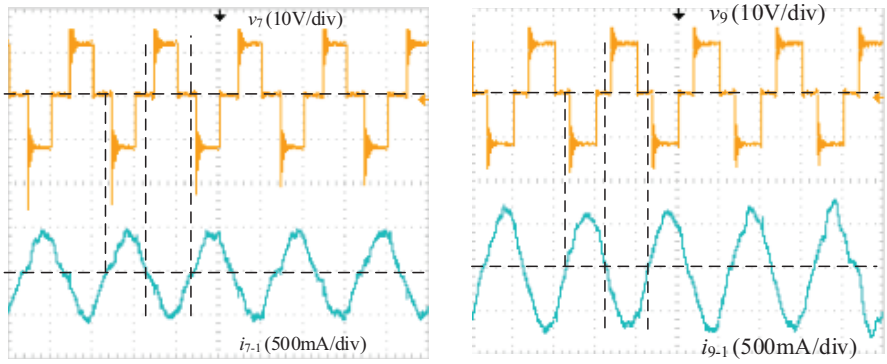

(a) Node 7; (b) Node 9

Figure 20. Inverter output voltages and charging currents of receiving nodes in one-to-two model.

5.3. Two-to-one model

Related parameters are shown in Table 6 according to the same principle of energy flow control in 3.2. Phase-shifting angles ϕ_3 and ϕ_4 are calculated to adjust the transmission power of transmitting nodes 3 and 4. Inverter output voltages and charging currents of transmitting nodes 3 and 4 are shown in Figure 21. In the real system, the transmission powers measured by the power analyzer are 0.98 W in node 3 and 1.96 W in node 4.

Table 6. Parameters for two-to-one model.

Node	Note	Value	
3	Residual energy	64 J	
	Transmission power	Theory	1 W
		Reality	0.98 W
	Phase-shifting angle ϕ_3	123°	
4	Residual energy	65 J	
	Transmission power	Theory	2 W
		Reality	1.96 W
	Phase-shifting angle ϕ_4	88.6°	
6	Residual energy	60 J	
	Phase-shifting angle ϕ_6	0°	

5.4. Relay-type model

Supposing 7-W power will be transmitted from node 1 to node 6 via node 4 in Figure 5, the phase-shifting angles ϕ_1 of node 1 equals 3.6° according to Eq. (22). The inverter output voltage and primary charging current of node 1 are shown in Figure 22. The transmission power of node 1 is 6.87 W in actual measurement by the power analyzer, which verifies the correctness of the control strategy for the relay-type model.

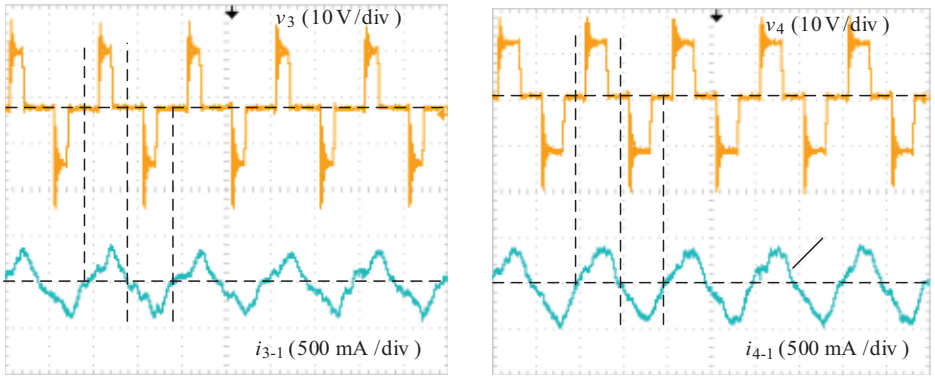

(a) Node 3; (b) Node 4

Figure 21. Inverter output voltages and charging currents of transmitting nodes in two-to-one model.

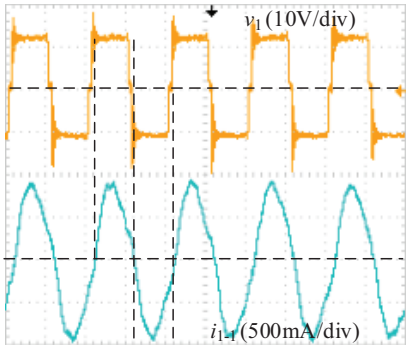

Figure 22. Inverter output voltage and charging current of node 1 in relay-type model.

6. Conclusion

A new type of WPTN for WSNs with bidirectional energy and signal transmission is proposed in this paper to prevent the premature death of WSNs. In particular, the path planning based on the Dijkstra algorithm is discussed in depth to achieve energy balance of WPTNs and minimize the overall energy consumption in the network to improve system efficiency. Besides, three basic energy models are summarized from WPTNs, and energy flow control strategy based on LCL topology is analyzed. Finally, the viability of the proposed method is supported by experiments.

Acknowledgments

This work was supported by the Natural Science Foundation of China (51307173) and the Postgraduate Research and Innovation Program of Jiangsu Province (SJLX16_0633).

References

[1] Akyildiz IF, Su W, Sankarasubramaniam Y, Cayirci E. Wireless sensor networks: a survey. Comput Netw 2002; 38: 393-422.

[2] Peng CH, Qian K, Wang CY. Design and application of a VOC-monitoring system based on a ZigBee wireless sensor network. IEEE Sens J 2017; 17: 2255-2268.

[3] Asaduzzaman, Kong HY. Energy efficient cooperative LEACH protocol for wireless sensor networks. J Commun Netw 2010; 12: 358-365.

[4] Younis O, Fahmy S. HEED: a hybrid, energy-efficient, distributed clustering approach for ad hoc sensor networks. IEEE T Mobile Comput 2004; 3: 366-379.

[5] Yan JJ, Zhou MC, Ding ZJ. Recent advances in energy-efficient routing protocols for wireless sensor networks: a review. IEEE Access 2016; 4: 5673-5686.

[6] Zhao M, Yang YY. Optimization-based distributed algorithms for mobile data gathering in wireless sensor networks. IEEE T Mobile Comput 2012; 11: 1464-1477.

[7] Wang C, Li J, Ye F, Yang YY. A mobile data gathering framework for wireless rechargeable sensor networks with vehicle movement costs and capacity constraints. IEEE T Comput 2016; 65: 2411-2427.

[8] Elliott GAJ, Raabe S, Covic GA, Boys JT. Multiphase pickups for large lateral tolerance contactless power transfer systems. IEEE T Ind Electron 2010; 57: 1590-1598.

[9] Liu X, Hui SY. Optimal design of a hybrid winding structure for planar contactless battery charging platform. IEEE T Power Electr 2008; 23: 455-463.

[10] Zhou SJ, Mi CC. Multi-paralleled LCC reactive power compensation networks and their tuning method for electric vehicle dynamic wireless charging. IEEE T Ind Electron 2016; 63: 6546-6556.

[11] Lee CH. Wireless information and power transfer for communication recovery in disaster areas. In: 2014 IEEE 15th International Symposium On a World of Wireless, Mobile and Multimedia Networks (WOWMOM); 16–19 June 2014; Sydney, Australia: IEEE. pp. 235-239.

[12] Li TS, Han Z, Ogai H, Sawada K, Wang J. A microchip-controlling wireless power transfer system for sensor network. In: 2012 SCIE Annual Conference; 20–23 August 2012; Akita University, Akita, Japan: IEEE. pp. 337-341.

[13] Zhao M, Li J, Yang YY. A framework of joint mobile energy replenishment and data gathering in wireless rechargeable sensor networks. IEEE T Mobile Comput 2014; 13: 2689-2705.

[14] He SB, Chen JM, Jiang FC, Yau DKY, Xing GL, Sun YX. Energy provisioning in wireless rechargeable sensor networks. IEEE T Mobile Comput 2013; 12: 1931-1942.

[15] Yan JJ, Zhou MC, Ding ZJ. Effects of practical recharge ability constraints on perpetual RF harvesting sensor network operation. IEEE Access 2016; 4: 750-765.

[16] Dijkstra EW. A note on two problems in connexion with graphs. J Numer Math 1959; 1: 269-271.